Journal of Dynamics, Monitoring and Diagnostics, 2023, 2, 177-182
https://doi.org/10.37965/jdmd.2023.151

ISTP
RESEARCH ARTICLE

Wind Turbine Planetary Gearbox Fault Diagnosis via Proportion-Extracting Synchrosqueezing Chirplet Transform

Dong Zhang and Zhipeng Feng
School of Mechanical Engineering, University of Science and Technology Beijing, Beijing, China

(Received 19 January 2023; Revised 09 May 2023; Accepted 11 July 2023; Published online 12 July 2023)

Abstract: Wind turbine planetary gearboxes usually work under time-varying conditions, leading to nonstationary vibration signals. These signals often consist of multiple time-varying components with close instantaneous frequencies. Therefore, high-quality time-frequency analysis (TFA) is needed to extract the time-frequency feature from such nonstationary signals for fault diagnosis. However, it is difficult to obtain high-quality time-frequency representations (TFRs) through conventional TFA methods due to low resolution and time-frequency blurs. To address this issue, we propose a new TFA method termed the proportion-extracting synchrosqueezing chirplet transform (PESCT). Firstly, the proportion-extracting chirplet transform is employed to generate high-resolution underlying TFRs. Then, the energy concentration of the underlying TFRs is enhanced via the synchrosqueezing transform. Finally, wind turbine planetary gearbox fault can be diagnosed by analysis of the dominant time-varying components revealed by the concentrated TFRs with high resolution. The proposed PESCT is suitable for achieving high-quality TFRs for complicated nonstationary signals. Numerical and experimental analyses validate the effectiveness of the PESCT in characterizing the nonstationary signals from wind turbine planetary gearboxes.

Keywords: nonstationary signal; planetary gearbox; synchrosqueezing transform; time-frequency analysis; wind turbine

I. INTRODUCTION

Planetary gearboxes are vital units in the drivelines of a wind turbine, and their running status directly affects the efficiency of the whole wind turbine system [1]. As they are prone to failures due to time-varying and tough operational environments, a lot of the cost of wind turbine maintenance involves planetary gearboxes [2]. Fortunately, conducting condition monitoring and fault diagnosis helps to avoid serious damage and unscheduled downtime and further reduce maintenance costs. The measured vibration signals carry rich information that contributes to recognizing the running status [3–5]. Thus, it is significant for such signals to develop an effective analysis method.

Wind turbines often operate under time-varying conditions, and the collected vibration signals from planetary gearboxes are composed of multiple time-varying and close-spaced components, which puts forward higher requirements for time-frequency analysis (TFA) methods. The vibration is excited by manufacturing errors, installing errors, gear meshing, rotating part failures, and so on. Hence, the collected nonstationary vibration signals feature multiple time-varying components [6]. The instantaneous frequencies (IFs) of these constituent components correspond to the characteristic frequencies (rotating frequency, fault characteristic frequency, and their harmonics or combinations) of the rotating parts, and they are often close to adjacent ones in the frequency domain. TFA has attracted considerable interest in processing nonstationary signals for revealing time-varying features of the constituent components [7]. For the multicomponent nonstationary signals, the frequency resolution of TFA methods must be less than the minimum intervals between constituent components, or the time-frequency representations (TFRs) get blurred. The blurry TFRs lead to difficulties in identifying the dominant components, estimating the running status, and locating faulty parts. Thus, we are left to high-resolution TFA methods.

Conventional TFA methods have extensive applications in nonstationary signal analysis, but they are insufficient to accurately reveal time-frequency signatures of the nonstationary signals with close-spaced IFs. For the linear time-frequency transforms, such as the short-time Fourier transform (STFT) and the continuous wavelet transform (CWT), their time-frequency resolutions depend on the predetermined parameters and cannot be arbitrarily improved due to the constraint of the Heisenberg uncertainty principle. Once the minimum IF intervals between the constituent components are smaller than the frequency resolution, the blurs occur in the STFT spectrogram and the CWT scalogram. In the TFRs obtained by bilinear transforms, such as the Wigner–Ville distribution, the cross-term interferences between adjacent components reduce their readability [8]. To improve the readability of the TFRs generated by the CWT, Daubechies et al. [9] proposed the wavelet synchrosqueezed transform (WSST). Oberlin et al. [10] extended the synchrosqueezed transform (SST) to the STFT framework and proposed the Fourier synchrosqueezed transform (FSST). Besides, other variants are proposed in [11–13]. The FSST and the WSST enhance the energy concentration of the TFRs obtained via the STFT and the CWT, but their time-frequency resolutions highly rely on the underlying TFRs [14,15]. However, the STFT

Corresponding author: Zhipeng Feng (email: fengzp@ustb.edu.cn).

and the CWT fail to discern the close-spaced components because of the limited resolution, thereby leading to blurs both in the underlying TFRs and postprocessing ones [16]. By separating constituent components via the Vold–Kalman filter, the time-frequency blurs can be removed. To improve the readability of the postprocessing TFRs fundamentally, it is essential to employ high-resolution TFRs as the underlying TFRs.

Unlike the above-mentioned TFA methods, parameterized TFA methods can achieve high-resolution TFRs [17]. The chirplet transform is capable of handling monocomponent signals or multicomponent signals with the same linear variation rates [18]. For the nonlinear frequency-modulated signals, Yang et al. [19] designed multiple kernel functions and proposed a general parameterized time-frequency transform (GPTFT) framework. However, although the CT and the GPTFT can generate high-resolution and accurate TFRs, they are not suitable for nonstationary multicomponent signals with different variation rates [20–22]. To compensate for this deficiency, we proposed the proportion-extracting chirplet transform (PECT) in [23]. The PECT can produce high-quality TFRs for the nonstationary signals with proportional IFs. But the time-frequency energy inevitably disperses around the time-frequency ridges due to the inner product nature. Thus, further enhancements to the PECT are needed.

Aiming at generating high-quality TFRs for the nonstationary signals from planetary gearboxes, we propose the proportion-extracting synchrosqueezing chirplet transform (PESCT) in this paper. On the one hand, we utilize the PECT to produce high-resolution and smear-free underlying TFRs. On the other hand, the time-frequency coefficients of the underlying TFRs are reassigned along the frequency direction by extending SST to the PECT framework. This makes the proposed PESCT first produce more accurate underlying TFRs with higher resolution and then concentrate the dispersed energy, thereby generating high-quality TFRs with fine readability. Thus, the PESCT has a satisfactory performance in analyzing the nonstationary signals from planetary gearboxes. Unlike the TFA methods proposed in [16], the PESCT extracts the time-frequency coefficients with high precision in the time-frequency domain.

This paper is organized as follows. Section II gives the background and the details of the proposed PESCT. Simulated verification is carried out in Section III. Section IV applies the PESCT to characterize wind turbine planetary gearbox nonstationary signals. Finally, Section V presents the conclusions.

II. PROPORTION-EXTRACTING SYNCHROSQUEEZING CHIRPLET TRANSFORM

A. PROPORTION-EXTRACTING CHIRPLET TRANSFORM

The PECT extends the GPTFT to multicomponent signal analyses by introducing proportion-extracting operators. For a measured vibration signal $x(t)$ corresponding time-varying rotational frequency $f_{\mathrm{r}}(t)$, the PECT contains two successive steps to calculate time-frequency coefficients. The first step is to construct proportion-kernelled functions $\widetilde{\kappa}_i(\tau)$ and proportion-extracting operator $\mathrm{PEO}_i(t,f)$ as:

$$\widetilde{\kappa}_i(\tau) = [(2i-1)\mu/2] \times \kappa_{\mathrm{r}}(\tau), \tag{1}$$

$$\mathrm{PEO}_i(t,f) = \begin{cases} 1, & |f - \widetilde{\kappa}_i'(\tau)|_{\tau=t}| < \mu f_{\mathrm{r}}(t)/2 \\ 0, & |f - \widetilde{\kappa}_i'(\tau)|_{\tau=t}| \geq \mu f_{\mathrm{r}}(t)/2 \end{cases}, \tag{2}$$

where $\widetilde{\kappa}_i'(\tau)$ denotes the first-order derivatives with respect to τ, μ determines the step size to discretize the continuous interval $[0,O_{\max}]$,

$$O_{\max} = f_{\mathrm{s}}/\{2 \times \max[f_{\mathrm{r}}(t)]\}, \tag{3}$$

f_{s} is the sampling frequency, $\kappa_{\mathrm{r}}(t)$ is approximated via

$$\kappa_{\mathrm{r}}(\tau) = \sum_{i=1}^{n} \frac{c_{l,i}}{i}(\tau - t_l)^i + \gamma_l, \qquad \tau \in [t_l, t_{l+1}], \tag{4}$$

$c_{l,i}$ denotes the polynomial coefficient, and

$$\begin{cases} \gamma_1 = 0, & l = 1 \\ \gamma_l = \gamma_{l-1} - \sum_{i=1}^{n} \frac{c_{l,i}}{i}(t_{l-1} - t_l)^i, & l > 1 \end{cases}. \tag{5}$$

The second step is to calculate sub-TFRs with well-matched kernel functions and reconstruct the TFR $T_{\mathrm{P}}(t,f)$ of the signal $x(t)$ by:

$$T_{\mathrm{P}}(t,f) = \sum_{i=1} T_{\mathrm{G}}[t,f;\widetilde{\kappa}_i(\tau)] \cdot \mathrm{PEO}_i(t,f), \tag{6}$$

where $T_{\mathrm{G}}[t,f;\widetilde{\kappa}_i(\tau)]$ is calculated by:

$$T_{\mathrm{G}}[t,f;\widetilde{\kappa}_i(\tau)] = \int_{-\infty}^{+\infty} z_s(\tau,t) w_\sigma^*(\tau - t) e^{-2\pi \mathrm{j} f \tau} \mathrm{d}\tau, \tag{7}$$

$\mathrm{j} = \sqrt{-1}$, w_σ is the Gaussian window function with a standard deviation σ, and $*$ denotes the complex conjugate. $z_s(\tau,t)$ is shifted and rotated by $\Phi_i^{\mathrm{R}}(\tau)$ and $\Phi_i^{\mathrm{S}}(\tau,t)$ as:

$$z_s(\tau,t) = x(\tau)\Phi_i^{\mathrm{R}}(\tau)\Phi_i^{\mathrm{S}}(\tau,t), \tag{8}$$

and

$$\begin{cases} \Phi_i^{\mathrm{R}}(\tau) = e^{\left[-2\pi \mathrm{j} \widetilde{\kappa}_i(\tau)\right]} \\ \Phi_i^{\mathrm{S}}(\tau,t) = e^{[2\pi \mathrm{j} \tau \widetilde{\kappa}_i'(\tau)|_{\tau=t}]} \end{cases}. \tag{9}$$

Compared with the GPTFT, the PECT can characterize the multicomponent nonstationary signals with different variation rates. The obtained TFRs are free of time-frequency blurs and achieve high resolutions. However, their time-frequency energy inevitably spreads around time-frequency ridges, since the PECT is to calculate the inner product between the windowed signal and the basis function. Thus, the PECT needs to be further enhanced to generate both high-resolution and concentrated TFRs.

B. PROPORTION-EXTRACTING SYNCHROSQUEEZING CHIRPLET TRANSFORM

To generate a smear-free and concentrated TFR, the FSST and the WSST assume that the constituent components are separated in the time-frequency domain. However, the STFT and the CWT cannot provide high-quality underlying TFRs for the nonstationary multicomponent signals with close-spaced IFs. Considering the merits of the PECT in achieving high-resolution underlying TFRs and the SST in sharpening underlying TFRs, we extend the SST to the PECT framework and propose the PESCT as (Fig. 1):

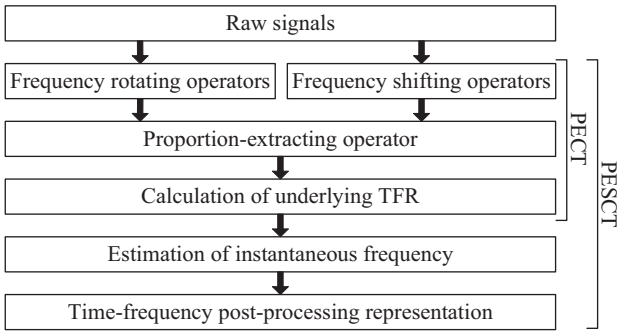

Fig. 1. Flowchart of PESCT.

$$\mathrm{SST}_{T_\mathrm{P}}(t,f') = \frac{1}{w_\sigma^*(0)} \int T_\mathrm{P}(t,f)\delta[f' - \widehat{f}(t,f)]\mathrm{d}f, \quad (10)$$

where

$$\delta[f' - \widehat{f}(t,f)] = \begin{cases} 1, & f' = \widehat{f}(t,f) \\ 0, & f' \neq \widehat{f}(t,f) \end{cases}. \quad (11)$$

and $\widehat{f}(t,f)$ is estimated by;

$$\widehat{f}(t,f) = \frac{1}{2\pi} \times \frac{\partial\{\arg[T_\mathrm{P}(t,f)]\}}{\partial t}. \quad (12)$$

The proposed PESCT has satisfactory performance in characterizing the frequency contents and associated amplitudes of the nonstationary signals with proportional IFs. This is because: (1) the frequency rotating operators address the spectral overlapping issues, and we can select a longer short-time window to ensure sufficient frequency resolution; (2) the frequency shifting operators guarantee the high time resolution; (3) the proportion-extracting operator removes the time-frequency blurs; and (4) the postprocessing procedure in the PESCT gathers the diffused time-frequency energy. As the time-frequency resolution and the energy concentration are improved simultaneously, the proposed PESCT obtains high-quality TFRs.

III. NUMERICAL VALIDATION

In this section, we employ a simulated signal to evaluate the effectiveness of the proposed PESCT. The simulated signal is formulated as:

$$x(t) = \sum_{i=1}^{5} A_i[1 - A\cos(2\pi f_\mathrm{M} t)] \times \cos\left[\int 2\pi O_i f_\mathrm{r}(t)\mathrm{d}t\right] + n(t), \quad (13)$$

where $A = 0.1$, $f_\mathrm{M}(t) = 0.05$ Hz, $t = (1,2,\ldots,2560)/256$, $f_\mathrm{r} = 16 - 8\sin(2\pi f_\mathrm{M} t + 0.9)$, $n(t)$ stands for the white Gaussian noise with a signal-to-noise ratio of 5 dB, and Table I lists the values of other parameters in the simulated signal model.

The waveform of the simulated signal is shown in Fig. 2(a). Figure 3 displays the analysis results using the conventional methods and the proposed PESCT. The STFT, the CWT, and the spline chirplet transform (SCT) fail to distinguish the 3rd, 4th, and 5th components due to the limited resolution (see Fig. 3(a), (e), and (i)). In the corresponding postprocessing TFRs via the SST, the energy concentration and readability are highly enhanced, but the two TFRs are blurry. Thanks to the high time-frequency resolution, the PECT discerns the three close-spaced components, but the dispersed time-frequency energy downgrades the readability. Benefitting from the high time-frequency resolution and concentrated energy, the TFR generated by the PESCT accurately captures the time-varying features of all constituent components (see Fig. 3(m), (n)). Figure 4 shows the rényi entropy to quantify the energy concentration of the obtained TFRs. Although the TFRs via the FSST and the WSST have smaller rényi entropy, the time-frequency blurs downgrade their readability. The proposed PESCT provides a more concentrated TFR than the PECT, and it achieves high time-frequency resolution. Thus, the PESCT is feasible for generating high-quality TFRs for complicated nonstationary signals.

Table I. Parameters in the simulated signal model

*i*th	1	2	3	4	5
A_i	2.00	2.00	2.50	2.00	2.50
O_i	0.50	1.00	1.85	2.00	2.15

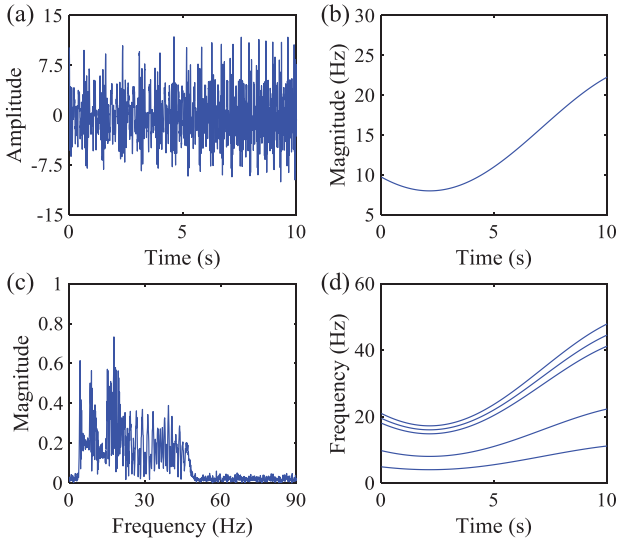

Fig. 2. Simulated signal: (a) waveform, (b) rotational frequency, (c) Fourier spectrum, and (d) true IF trajectories.

IV. APPLICATION TO WIND TURBINE PLANETARY GEARBOX SIGNAL ANALYSIS

In this section, the vibration signals from a wind turbine planetary gearbox test rig are used to validate the practicability of the proposed PESCT.

A. EXPERIMENTAL SETTING

Figure 5 shows the planetary gearbox test rig. The test rig comprises a driving motor, a fixed-shaft gearbox, two planetary gearboxes, a brake, two accelerometers, and a tachometer. Refer to [16] for the specific parameters of the test rig. It mimics the wind turbine drivetrain. The rotational frequency of the driving motor increases from 20 Hz to 40 Hz, and the rotational frequency of the brake rises from 9.72 RPM to 19.44 RPM, thereby covering the commonly

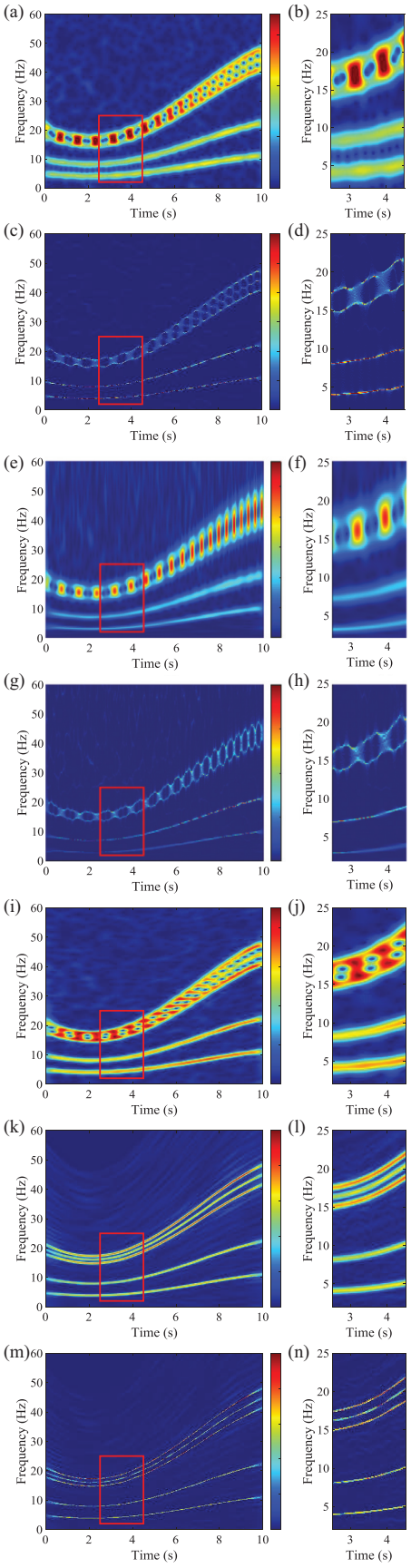

Fig. 3. TFRs obtained via: (a) STFT, (b) close-up of STFT, (c) FSST, (d) close-up of FSST, (e) CWT, (f) close-up of CWT, (g) WSST, (h) close-up of WSST, (i) SCT, (j) close-up of SCT, (k) PECT, (l) close-up of PECT, (m) PESCT, and (n) close-up of PESCT.

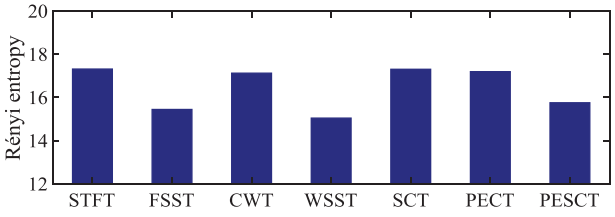

Fig. 4. Rényi entropy.

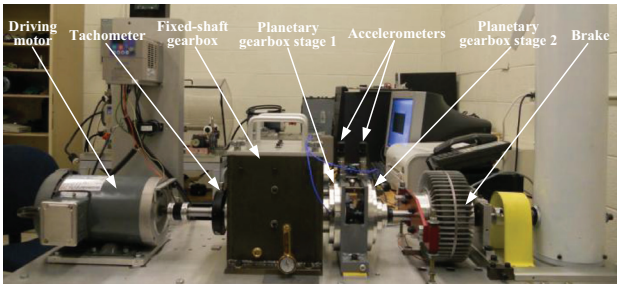

Fig. 5. Wind turbine planetary gearbox test rig.

used cut-in and cut-out speed of wind turbines (see Fig. 6). The vibration signals and the rotational frequency of the driving motor are simultaneously recorded by two accelerometers fixed on the gearbox casing and a tachometer, with a sampling frequency of 20k Hz. We conducted two sets of experiments: baseline case and stage 1 sun gear wear case (see Fig. 7). We analyze herein the vibration signal

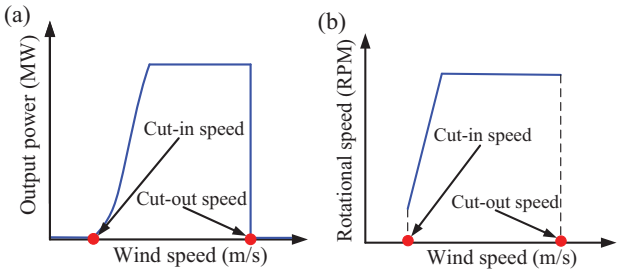

Fig. 6. Wind turbine power curve.

Fig. 7. Stage 1 sun gear wear.

recorded by the accelerometer fixed on the planetary gearbox stage 1.

B. PLANETARY GEARBOX VIBRATION SIGNAL ANALYSIS

Figure 8 displays the waveform of the baseline vibration signal and the driving motor rotational frequency f_d. The PESCT discerns three dominant time-varying components, that is, $2f_d, f_{m1} - 3f_{s1}^{(r)}$, and $f_{m1} + f_{s1}^{(r)}$ (the combinations of the stage 1 meshing frequency f_{m1} and sun gear rotational frequency $f_{s1}^{(r)}$), as shown in Fig. 9. Any fault characteristic frequency does not exist, thereby indicating that stage 1 planetary gearbox is normal.

In the stage 1 sun gear wear case, the waveform of the measured vibration signal and the corresponding driving motor rotational frequency are shown in Fig. 10(a) and (b). In Fig. 11, the PESCT provides a high-resolution TFR and

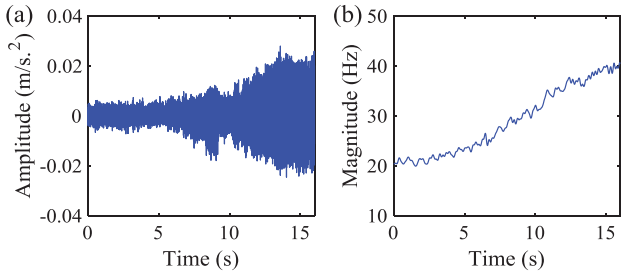

Fig. 8. Planetary gearbox baseline signals: (a) waveform and (b) driving motor rotational frequency.

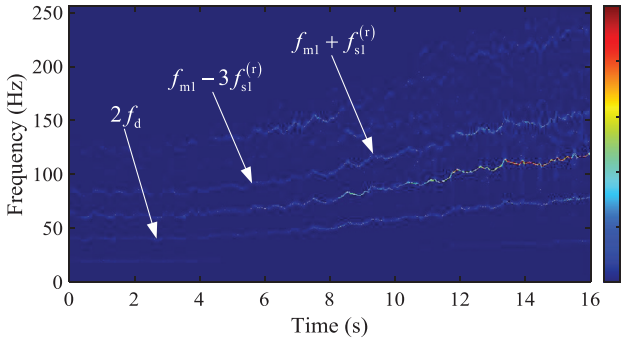

Fig. 9. The TFR of the planetary gearbox baseline vibration signal via PESCT.

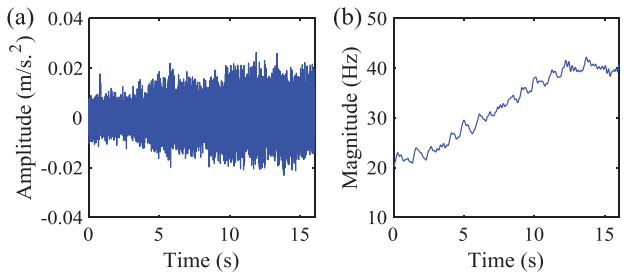

Fig. 10. Planetary gearbox sun gear wear signals: (a) waveform and (b) drive motor rotational frequency.

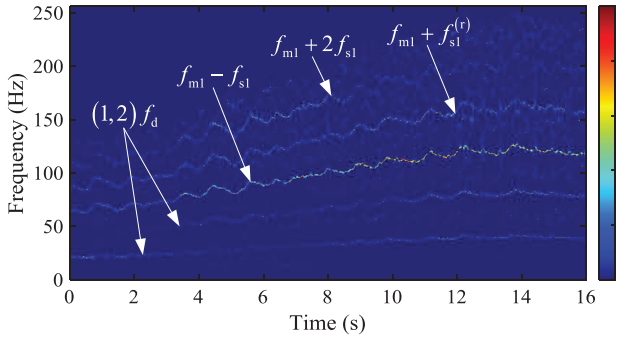

Fig. 11. The TFR of the planetary gearbox sun gear wear vibration signal via PESCT.

perceives five dominant time-varying components. Compared with the TFR in the baseline case, there exist three new components, that is, f_d, time-varying sidebands $f_{m1} - f_{s1}$ and $f_{m1} + 2f_{s1}$ around the stage 1 meshing frequency f_{m1}. The sidebands corresponding to the stage 1 sun gear fault characteristic frequency are the obvious sign of stage 1 sun gear fault.

V. CONCLUSIONS

In this paper, we propose a high-resolution TFA method termed the PESCT by extending the SST to the PECT framework. The proposed PESCT shows success in generating high-resolution TFRs with concentrated energy for the nonstationary signals from a wind turbine planetary gearbox. The proposed PESCT first employs smear-free and high-resolution underlying TFRs generated by the PECT and then gathers the dispersed energy via time-frequency postprocessing. This enables the PESCT to gain superior performances in terms of both time-frequency resolution and energy concentration. One numerical and two experimental datasets of a wind turbine planetary gearbox are selected to evaluate the performance of the proposed PESCT. The analysis results validate the effectiveness and superiority of the PESCT in the analysis of nonstationary signals with complicated time-frequency structures.

ACKNOWLEDGMENTS

This work was supported by the National Natural Science Foundation of China (52275080). The authors are grateful to the reviewers for their valuable comments.

CONFLICT OF INTEREST STATEMENT

Zhipeng Feng is a guest editor for the special issue on Monitoring and Diagnostics of Renewable Energy System for the *Journal of Dynamics, Monitoring and Diagnostics*, and he was not involved in the editorial review or the decision to publish this article. The authors declare that they have no conflict of interest.

REFERENCES

[1] T. Y. Wang, Q. K. Han, F. L. Chu, and Z. P. Feng, "Vibration based condition monitoring and fault diagnosis of wind

turbine planetary gearbox: a review," *Mech. Syst. Signal Process.*, vol. 126, pp. 662–685, 2019.

[2] M. Hilbert, W. A. Smith, and R. B. Randall, "The effect of signal propagation delay on the measured vibration in planetary gearboxes," *J. Dyn. Monit. Diagn.*, vol. 1, no. 1, pp. 9–18, 2022.

[3] H. X. Zhou, X. Huang, G. R. Wen, Z. H. Lei, S. Z. Dong, P. Zhang, and X. F. Chen, "Construction of health indicators for condition monitoring of rotating machinery: a review of the research," *Exp. Syst. Appl.*, vol. 203, Art. no. 117297, 2022.

[4] B. Y. Chen, D. L. Song, Y. Cheng, W. H. Zhang, B. S. Huang, and Y. Muhamedsalih, "IGIgram: an improved Gini index-based envelope analysis for rolling bearing fault diagnosis," *J. Dyn. Monit. Diagn.*, vol. 1, no. 2, pp. 111–124, 2022.

[5] Y. D. Xu, X. L. Tang, G. J. Feng, D. Wang, C. Ashworth, F. S. Gu, and A. Ball, "Orthogonal on-rotor sensing vibrations for condition monitoring of rotating machines," *J. Dyn. Monit. Diagn.*, vol. 1, no. 1, pp. 29–36, 2022.

[6] Y. H. Miao, M. Zhao, V. Makis, and J. Lin, "Optimal swarm decomposition with whale optimization algorithm for weak feature extraction from multicomponent modulation signal," *Mech. Syst. Signal Process.*, vol. 122, pp. 673–691, 2019.

[7] Z. P. Feng, M. Liang, and F. L. Chu, "Recent advances in time-frequency analysis methods for machinery fault diagnosis: a review with application examples," *Mech. Syst. Signal Process.*, vol. 38, no. 1, pp. 165–205, 2013.

[8] F. Hlawatsch and G. F. Boudreaux-Bartels, "Linear and quadratic time-frequency signal representations," *IEEE Signal Process. Mag.*, vol. 9, no. 2, pp. 21–67, 1992.

[9] I. Daubechies, J. Lu, and H. T. Wu, "Synchrosqueezed wavelet transforms: an empirical mode decomposition-like tool," *Appl. Comput. Harmon. Anal.*, vol. 30, no. 2, pp. 243–261, 2011.

[10] T. Oberlin, S. Meignen, and V. Perrier, "The Fourier-based synchrosqueezing transform," in *2014 IEEE Int. Conf. Acoust. Speech Signal Process. (ICASSP)*, Florence, Italy, May 2014, pp. 315–319.

[11] G. Yu, Z. H. Wang, and P. Zhao, "Multisynchrosqueezing transform," *IEEE Trans. Ind. Electron.*, vol. 66, no. 7, pp. 5441–5455, 2019.

[12] Y. Hu, X. T. Tu, and F. C. Li, "High-order synchrosqueezing wavelet transform and application to planetary gearbox fault diagnosis," *Mech. Syst. Signal Process.*, vol. 131, pp. 126–151, 2019.

[13] S. Meignen, T. Oberlin, and D. H. Pham, "Synchrosqueezing transforms: from low- to high-frequency modulations and perspectives," *C. R. Phys.*, vol. 20, no. 5, pp. 449–460, 2019.

[14] G. Thakur, E. Brevdo, N. S. Fuckar, and H. T. Wu, "The synchrosqueezing algorithm for time-varying spectral analysis: robustness properties and new paleoclimate applications," *Signal Process.*, vol. 93, no. 5, pp. 1079–1094, 2013.

[15] D. Iatsenko, P. V. E. McClintock, and A. Stefanovska, "Linear and synchrosqueezed time-frequency representations revisited: overview, standards of use, resolution, reconstruction, concentration, and algorithms," *Digital Signal Process.*, vol. 42, pp. 1–26, 2015.

[16] D. Zhang and Z. P. Feng, "Enhancement of time-frequency post-processing readability for nonstationary signal analysis of rotating machinery: principle and validation," *Mech. Syst. Signal Process.*, vol. 163, Art. no. 108145, 2022.

[17] Y. Yang, Z. K. Peng, W. M. Zhang, and G. Meng, "Parameterised time-frequency analysis methods and their engineering applications: a review of recent advances," *Mech. Syst. Signal Process.*, vol. 119, pp. 182–221, 2019.

[18] S. Mann and S. Haykin, "The chirplet transform: physical considerations," *IEEE Trans. Signal Process.*, vol. 43, no. 11, pp. 2745–2761, 1995.

[19] Y. Yang, Z. K. Peng, X. J. Dong, W. M. Zhang, and G. Meng, "General parameterized time-frequency transform," *IEEE Trans. Signal Process.*, vol. 62, no. 11, pp. 2751–2764, 2014.

[20] Y. Yang, X. J. Dong, Z. K. Peng, W. M. Zhang, and G. Meng, "Vibration signal analysis using parameterized time-frequency method for features extraction of varying-speed rotary machinery," *J. Sound Vib.*, vol. 335, pp. 350–366, 2015.

[21] Y. Yang, W. M. Zhang, Z. K. Peng, and G. Meng, "Multicomponent signal analysis based on polynomial chirplet transform," *IEEE Trans. Ind. Electron.*, vol. 60, no. 9, pp. 3948–3956, 2013.

[22] K. Yu, T. R. Lin, H. Ma, H. F. Li, and J. Zeng, "A combined polynomial chirplet transform and synchroextracting technique for analyzing nonstationary signals of rotating machinery," *IEEE Trans. Instrum. Meas.*, vol. 69, no. 4, pp. 1505–1518, 2020.

[23] D. Zhang and Z. P. Feng, "Proportion-extracting chirplet transform for nonstationary signal analysis of rotating machinery," *IEEE Trans. Ind. Informat.*, vol. 19, no. 3, 2023.